university of groningen

University Medical Center Groningen

University of Groningen

ZnO nanorod arrays assembled on activated carbon fibers for photocatalytic degradation

Luo, Sha; Liu, Chunwei; Zhou, Sui; Li, Wei; Ma, Chunhui; Liu, Shouxin; Yin, Wang; Heeres, Hero Jan; Zheng, Weiqing; Seshan, Kulathuiyer

Published in:
Chemosphere

DOI:
10.1016/j.chemosphere.2020.127731

IMPORTANT NOTE: You are advised to consult the publisher's version (publisher's PDF) if you wish to cite from it. Please check the document version below.

Document Version
Publisher's PDF, also known as Version of record

Publication date:
2020

Link to publication in University of Groningen/UMCG research database

Citation for published version (APA):
Luo, S., Liu, C., Zhou, S., Li, W., Ma, C., Liu, S., Yin, W., Heeres, H. J., Zheng, W., Seshan, K., & He, S. (2020). ZnO nanorod arrays assembled on activated carbon fibers for photocatalytic degradation: Characteristics and synergistic effects. *Chemosphere*, *261*, [127731]. https://doi.org/10.1016/j.chemosphere.2020.127731

Copyright
Other than for strictly personal use, it is not permitted to download or to forward/distribute the text or part of it without the consent of the author(s) and/or copyright holder(s), unless the work is under an open content license (like Creative Commons).

The publication may also be distributed here under the terms of Article 25fa of the Dutch Copyright Act, indicated by the “Taverne” license. More information can be found on the University of Groningen website: https://www.rug.nl/library/open-access/self-archiving-pure/taverne-amendment.

Take-down policy
If you believe that this document breaches copyright please contact us providing details, and we will remove access to the work immediately and investigate your claim.

Downloaded from the University of Groningen/UMCG research database (Pure): http://www.rug.nl/research/portal. For technical reasons the number of authors shown on this cover page is limited to 10 maximum.

Download date: 05-06-2022

Chemosphere 261 (2020) 127731

Contents lists available at ScienceDirect

Chemosphere

journal homepage: www.elsevier.com/locate/chemosphere

ZnO nanorod arrays assembled on activated carbon fibers for photocatalytic degradation: Characteristics and synergistic effects

Sha Luo [a], Chunwei Liu [a], Sui Zhou [a], Wei Li [a, *], Chunhui Ma [a], Shouxin Liu [a, **], Wang Yin [b], Hero Jan Heeres [b], Weiqing Zheng [c], Kulathuiyer Seshan [d], Songbo He [b, ***]

[a] Key Laboratory of Bio-based Material Science and Technology of Ministry of Education, College of Material Science and Engineering, Northeast Forestry University, Harbin, 150040, PR China
[b] Green Chemical Reaction Engineering, Engineering and Technology Institute Groningen, University of Groningen, Nijenborgh 4, 9747, AG Groningen, the Netherlands
[c] Catalysis Center for Energy Innovation and Center for Catalytic Science and Technology, Department of Chemical and Biomolecular Engineering, University of Delaware, Newark, DE, 19716, USA
[d] Faculty of Science and Technology, University of Twente, 7500, AE Enschede, the Netherlands

HIGHLIGHTS

- MB adsorbability per surface area of the synthesized ZnO NRAs is 39% of that of ACFs.
- MB adsorbtion on ZnO NRAs/ACFs increases linearly with surface area.
- Defect level of ZnO NRAs plays more role than other characteristics in TOF of ZnO NRAs/ACFs.
- ZnO NRAs/ACFs show higher synergistic effect than the mechanically mixed ZnO-ACFs.
- ZnO NRAs/ACFs after 5 recycles show comparable TOF with that for the fresh ZnO NRAs.

GRAPHICAL ABSTRACT

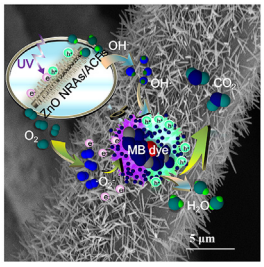

ARTICLE INFO

Article history:
Received 7 June 2020
Received in revised form
14 July 2020
Accepted 15 July 2020
Available online 24 July 2020

Handling Editor: Jun Huang

Keywords:
Adsorbability
TOF
Mineralization
Defect level

ABSTRACT

Well-aligned ZnO nanorod arrays were assembled on activated carbon fibers by a stepwise sequence of sol-gel and hydrothermal synthesis methods. These ZnO nanorod arrays on activated carbon fibers having different characteristics such as surface area, rod concentration, aspect ratio and defect level, were applied as catalysts for the photodegradation of an aqueous methylene blue solution. They showed very promising methylene blue adsorbility in the dark (*ca.* 0.025–0.031 mg methylene blue m^{-2} catalyst, *vs.* 0.072 mg methylene blue m^{-2} activated carbon fibers). Significantly, the defect level of ZnO nanorod arrays has a major effect on the turnover frequency compared to other characteristics. A synergistic effect between activated carbon fibers and ZnO nanocrystals on enhancing turnover frequency was more significant for the well-assembled ZnO nanorod arrays on activated carbon fibers catalysts compared to the mechanically mixed ZnO powder with activated carbon fibers catalyst. Further, turnover frequency for the ZnO nanorod arrays on activated carbon fibers (0.00312 $mol_{methylene\ blue}\ mol_{ZnO}^{-1}\ h^{-1}$) was twice higher than that for the corresponding bare ZnO nanorod arrays, and 3 times higher than that for a commercial ZnO powder. In addition, ZnO nanorod arrays on activated carbon fibers show high

* Corresponding author.
** Corresponding author.
*** Corresponding author.
E-mail addresses: liwei19820927@126.com (W. Li), liushouxin@126.com (S. Liu), songbo.he@rug.nl (S. He).

https://doi.org/10.1016/j.chemosphere.2020.127731
0045-6535/© 2020 The Author(s). Published by Elsevier Ltd. This is an open access article under the CC BY license (http://creativecommons.org/licenses/by/4.0/).

Photocatalysis
Synergistic effect

degradation (77.5%) and mineralization (55.0%) levels for methylene blue, and also good reusability (or stability) as demonstrated by a sequential 5-time recycle routine. These outstanding features indicate that activated carbon fibers supported ZnO nanorod arrays have significant potential to be used as catalysts for photodegradation.
© 2020 The Author(s). Published by Elsevier Ltd. This is an open access article under the CC BY license (http://creativecommons.org/licenses/by/4.0/).

1. Introduction

ZnO is regarded as an alternative photocatalyst (Chakrabarti and Dutta, 2004) for photocatalytic treatment of wastewater, in which TiO_2 is commonly employed (Feng et al., 2014). ZnO nanocrystals with different morphologies (*e.g.*, nanopowder (Lv et al., 2016), nanofibers (Panthi et al., 2015), nanotubes (Bojer et al., 2017), nanoflowers (Lam et al., 2018a, 2018b), nanoflakes (Zhang et al., 2019) and nanorods (Xu et al., 2018)) have been applied for photocatalytic degradation of wastewater particularly containing organic dyes (*e.g.*, Methylene Blue (Ummartyotin and Pechyen, 2016; Nguyen et al., 2019), Eosin Y (Chakrabarti and Dutta, 2004), Acid Yellow 23 (Modirshahla et al., 2011), Acid Orange 7 (Xu et al., 2018), Rhodamine B (Lv et al., 2016; Nguyen et al., 2019), Ponceau S (Marathe and Shrivastava, 2015) and Malachite Green (Lam et al., 2018a, 2018b)). In some reports, ZnO nanocomposites with *e.g.*, Al_2O_3 (Park et al., 2007), clay (Mustapha et al., 2020), Fe_2O_3 (Al Haiqi et al., 2020) and MgO (Raj et al., 2019), were also applied to achieve enhanced photocatalytic degradation efficiency. The effect of ZnO characteristics such as crystal size and facet (McLaren et al., 2009), aspect ratio (rod length/rod diameter) (Zhang et al., 2014), surface area (Melian et al., 2009) and defect level (Wang et al., 2009), have also been extensively investigated.

Nevertheless, these ZnO nanoparticles/nanocomposites tend to agglomerate and are difficult to recover from the treated solution (Lu et al., 2008; Thi and Lee, 2017). One of the practical solutions is to immobilize or anchor ZnO to substrates, such as glass (Vaiano and Iervolino, 2018), reduced graphene oxide (Nguyen et al., 2019; Fan et al., 2015), Nylon 6 (Ummartyotin and Pechyen, 2016), carbonized oak (Tafreshi et al., 2019) and activated carbon (Melian et al., 2009; Raizada et al., 2014). Among these reported substrates, activated carbon materials are particularly attractive and synergistic effects have been observed on photocatalytic degradation efficiency of supported or mixed ZnO catalysts. This is achieved by (i) providing large surface areas for enhanced adsorption of reactants on the catalyst surface, (ii) improving the separation of photo generated electron/hole (e^-/h^+) pairs, (iii) increasing the light harvesting efficiency and (iv) narrowing the band-gap of ZnO (Melian et al., 2009; Raizada et al., 2014; Byrappa et al., 2006; Sobana and Swaminathan, 2007; Vinayagam et al., 2018). Furthermore, carbon materials were also reported to suppress the photocorrosion of ZnO/Carbon nanoparticles during reaction (Zhang et al., 2009).

Flexible activated carbon fibers (ACFs) with favorable properties like large surface area, high adsorbability and convenience in handling (Tian et al., 2017; Liu et al., 2018), have also been considered for the immobilization of ZnO nanocrystals. Chen et al. immobilized ZnO nanoflowers (ZnO NFs) on ACFs by a hydrothermal method and reported an improved photocatalytic degradation of dyes (Chen et al., 2014) combined with a good catalyst recyclability (Chen et al., 2016). Thi et al. fabricated ZnO rod on activated carbon fiber (ZnO rod-ACF) by a 'microwave method', which was based on a hydrothermal synthesis approach with an additional ZnO seed formation step (Thi and Lee, 2017). The ZnO rod-ACF composites showed a higher total organic carbon (TOC) removal than bare ZnO. Recently, the authors have successfully assembled ZnO nanorod arrays (ZnO NRAs) on ACFs (ZnO NRAs/ACFs) by an integrated sol-gel and hydrothermal synthesis method (Luo et al., 2020). The well-aligned ZnO NRAs showed extremely high surface area (20 $m^2\ g^{-1}$), aspect ratio (20:1) and defect level. A preliminary evaluation of ZnO NRAs/ACFs for the photocatalytic degradation of methylene blue (MB) showed excellent MB degradation (77.5%) (Luo et al., 2020). However, due to the different reaction conditions used such as MB concentration and ZnO dosage, it is not straightforward to compare the novel ZnO NRAs assembled on ACFs with state-of-the-art ZnO nanocrystals and to obtain insights in synergistic effects, if any, on the novel ZnO NRAs/ACFs catalysts.

In this contribution, the turnover frequency (TOF) of the catalyst has been used as a parameter for the evaluation of photocatalytic degradation efficiency of the novel ZnO NRAs and ZnO NRAs/ACFs catalysts. TOF is widely used to evaluate catalyst efficiency but has not been considered for photocatalytic degradation. ZnO NRAs/ACFs catalysts with different characteristics such as surface area, aspect ratio, rod concentration and defect level, were studied for photocatalytic degradation of aqueous methylene blue solution. Each characteristic has been investigated in detail aiming to establish the effect of the structural and optical characteristics of the ZnO NRAs/ACFs on photocatalytic degradation performance. All these aspects have been discussed in the existing literature separately but never in a systematic and comprehensive manner. Bare ZnO powder, nanorods (NRs) and nanorod arrays (NRAs) were also tested to study possible synergistic effect between ACFs and three types of ZnO nanocrystals. By eliminating differences in reaction conditions (*vide supra*) and the use of the TOF as a measure for catalyst activity, possible synergistic effect between ACFs and ZnO nanoparticles can be established more accurately. Finally, catalyst reusability (or stability) was checked by performing recycle experiments in batch for 5 times. The results provide insights in the effects of catalyst structure as well as synergistic effects on photocatalytic degradation when using well-aligned ZnO nanorod arrays on activated carbon fibers.

2. Experimental

2.1. Materials

Activated carbon fibers (surface area of 940 $m^2\ g^{-1}$ (Luo et al., 2020)) were supplied by Qinhuangdao Zichuan Carbon Fiber Co., Ltd., PR China. ZnO powder (surface area of 4 $m^2\ g^{-1}$ (Luo et al., 2020)), methylene blue ($C_{16}H_{18}ClN_3S$) and all the chemicals used for the syntheses of the catalysts, namely zinc acetate dihydrate ($Zn(CH_3COO)_2{\cdot}2H_2O$), 2-methoxyethanol ($CH_3OCH_2CH_2OH$), monoethanolamine (MEA, $HOCH_2CH_2NH_2$), zinc nitrate hexahydrate ($Zn(NO_3)_2{\cdot}6H_2O$), hexamethylenetetramine (HMT, $(CH_2)_6N_4$) and absolute ethanol (CH_3CH_2OH), were of analytical grade and supplied by Tianjin Kemiou Chemical Reagent Co., Ltd., PR China.

2.2. Catalyst preparation

An integrated synthesis approach involving a sol-gel (Ohyama et al., 1997) followed by a hydrothermal synthesis step (Vayssieres, 2003) has been reported by the authors (Luo et al., 2020) to assemble well-aligned ZnO nanorod arrays on ACFs. In the first step, a layer of ZnO seeds (denoted as ZnO SLs) was precipitated on the ACFs surface. Zinc acetate dihydrate (1.10–2.74 g, equivalent to 0.1–0.25 mol L^{-1}) was dissolved in 2-methoxyethanol (50 mL) followed by adding MEA (0.3–0.75 mL) under stirring (400 rpm) at 60 °C. After 30 min, ACFs (3 × 3 cm) were added to the sol solution using a dip-coating protocol (Mechiakh et al., 2010). The wet ACFs with coating were dried under air at 80 °C for 12 h and then heated under N_2 at 500 °C for 10 min. The samples are denoted as ZnO SLs/ACFs-x with x being the zinc acetate concentration (mol L^{-1}) applied in the sol-gel synthesis step.

The hydrothermal synthesis solution was prepared by mixing a zinc nitrate solution (0.01–0.1 mol L^{-1}, 30 mL) and an HMT solution (0.01–0.1 mol L^{-1}, 30 mL) under stirring at 25 °C. After 30 min, the thus obtained solution together with the ZnO SLs/ACFs-x from the sol-gel synthesis step were loaded into a Teflon-lined stainless steel autoclave and heated to 95 °C for 1–6 h. Then after filtering, the filter cake was rinsed with deionized water (5 times) and then with ethanol (5 times). The wet samples were dried under air at 80 °C for 12 h to obtain ZnO nanorod arrays (denoted as ZnO NRAs) assembled on ACFs, which are denoted as ZnO NRAs/ACFs-x-y-z with y being the zinc nitrate concentration (mol L^{-1}) and z the hydrothermal synthesis time (h).

By varying the concentrations of zinc acetate (x), zinc nitrate (y) and hydrothermal synthesis time (z), in total, 9 ZnO NRAs/ACFs-x-y-z catalysts were prepared. For comparison, another catalyst, with ZnO nanorods (denoted as ZnO NRs) on ACFs, was synthesized by following the above protocol but using only 0.025 mol L^{-1} zinc nitrate hexahydrate and pristine ACFs for hydrothermal synthesis of 4 h. Accordingly, this catalyst is denoted as ZnO NRs/ACFs-0-0.025-4. In addition, a mechanically mixed catalyst consisting of commercial ZnO powder and ACFs (denoted as ZnO-ACFs) was also prepared.

Furthermore, for characterization and evaluation, bare ZnO nanocrystals (*vide infra*), ZnO NRs and ZnO NRAs samples were obtained by ultrasonicating the parent ZnO NRAs/ACFs-x-y-z and ZnO NRs/ACFs-0-0.025-4.

2.3. Catalyst characterization

Scanning electron microscopy (SEM) images were taken on ESEM Quanta 200 (FEI) equipped with PV7760/68 ME detector for energy dispersive X-ray (EDX) analysis. Samples were pasted onto the sample stage using conductive tape, followed by a gold sputtering treatment.

High resolution transmission electron microscopy (TEM) images and selected area electron diffraction (SAED) patterns were taken on Tecnai G2 F20 S-TWIN (FEI). The samples were uniformly dispersed in ethanol under ultrasonication, and subsequently loaded onto copper grids.

Physisorption of N_2 at 77 K was performed on ASAP 2020 (Micromeritics). Samples were degassed at 200 °C for 2 h under vacuum prior to measurements.

Photoluminescence (PL) spectra were recorded on FLS 980 (EI) at room temperature. The excitation wavelength was set at 325 nm. Samples were coated onto quartz cuvettes for solid fluorescence testing.

2.4. Photocatalytic degradation of MB

Photocatalytic degradation performance of the catalysts for the removal of dyes in aqueous solution was evaluated using MB as a model compound. Reactions were carried out in a jacketed glass reactor equipped with a UV lamp (365 nm, 8 W). The catalyst was added to the MB solution in the reactor and was magnetically stirred in the dark at 25 °C for 2 h (dark adsorption step). Afterwards, UV light was turned on and the photocatalytic degradation of MB was performed at 25 °C, during which the reaction solution was sampled every 20 min. A fixed temperature of 25 °C was applied in this contribution as this is the most common reaction temperature for photocatalytic degradation in the open publications. For a wider application, other reaction temperatures can also be considered. Detailed reaction parameters such as amount of MB solution, MB concentration before and after dark adsorption, catalyst dosage and reaction time, are shown in Tables S1, S3 and S4. ZnO dosage/ZnO loading on catalyst was fine tuned to ensure a similar MB concentration for each experiment after dark adsorption. As such, turnover frequency's (TOFs) of catalysts were applied for comparison of photocatalytic degradation efficiencies of the various catalysts.

MB concentrations in the samples were analyzed by TU 1950 UV–Vis spectrophotometry (PuXi, PR China). The concentrations of MB after 2-h dark adsorption were defined as the initial MB concentrations for the photocatalytic degradation experiments. Total organic carbon (TOC) values were analyzed using TOC-VCPN Analyzer (Shimadzu, Japan). The percentage degradation of MB (η), the mineralization of MB and the average turnover frequency of the catalyst were calculated using Equations (1)–(3) below.

$$MB\ \text{degradation}(\eta,\%) = \left(1 - \frac{MB\ concentration\ in\ the\ sample}{MB\ concentration\ after\ dark\ adsorption}\right) \times 100 \quad (1)$$

$$MB\ \text{mineralization}(\%) = \left(1 - \frac{TOC\ after\ 2-h\ photocatalytic\ \text{degradation}}{TOC\ after\ dark\ adsorption}\right) \times 100 \quad (2)$$

$$Average\ TOF\ \left(h^{-1}\right) = \left(\frac{moles\ of\ MB\ \text{degradaded during the reaction with UV light}}{moles\ of\ ZnO\ dose}\right) \Big/ reaction\ time \quad (3)$$

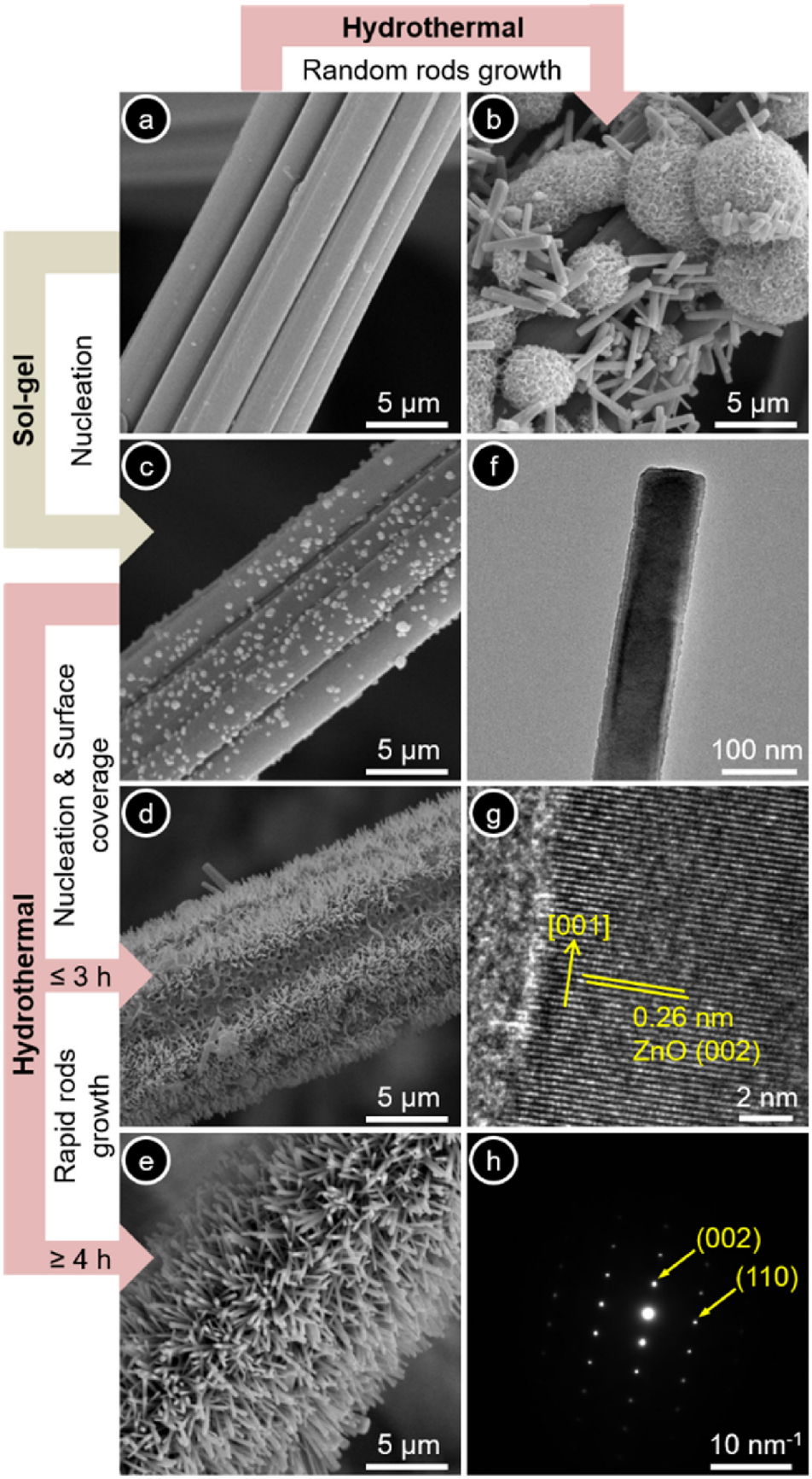

Fig. 1. SEM images of (a) ACFs, (b) ZnO NRs/ACFs, (c) ZnO SLs/ACFs, (d) ZnO NRAs/ACFs after hydrothermal synthesis of 3 h, (e) ZnO NRAs/ACFs after hydrothermal synthesis of 4 h, (f) TEM and (g) HRTEM images, and (h) SAED patterns of ZnO nanorod peeled off from ZnO NRAs/ACFs after hydrothermal synthesis of 4 h.

3. Results and discussions

3.1. Characteristics of the ZnO NRAs/ACFs

ZnO NRAs/ACFs catalysts were prepared by a stepwise approach developed earlier by the authors (Luo et al., 2020), which involves coating of ACFs with ZnO seed layers (ZnO SLs) *via* a sol-gel synthesis followed by growth of the well-aligned ZnO nanorod arrays (ZnO NRAs) *via* a hydrothermal synthesis step (Experimental Section 2.2). Pre-coating ZnO SLs on ACFs was of prime importance as evidenced by the formation of randomly assembled ZnO nanorods (ZnO NRs) and tufted spheres on the ACFs surface (Fig. 1-b) when only hydrothermal synthesis protocol using pristine ACFs (Fig. 1-a) was applied. The sol-gel synthesis step for the nucleation of ZnO SLs on ACFs included successive hydrolysis, condensation and annealing (Experimental Section 2.2). The obtained ZnO SLs on ACFs were shown to consist of relatively homogeneously mono-layer dispersed nanospheres with particle sizes between 150 and 250 nm (Fig. 1-c). It has been shown in our previous publication that the ZnO seed concentration may be tuned by adjusting the zinc acetate concentration during the sol-gel synthesis step (Luo et al., 2020). In the subsequent hydrothermal synthesis step, ZnO NRAs grow in an orderly fashion *via* simultaneous nucleation and surface coverage, and a successive rapid growth of the rods (Fig. 1). In the initial stage of the hydrothermal synthesis ($\leq$3 h), the ZnO nanorod growth rate is rather low and predominantly ZnO nanocrystalline grains are formed on the ACFs surface (Fig. 1-d). Prolongation of the hydrothermal synthesis time to 4 h leads to rapid growth of well-aligned NRAs on ACFs (Fig. 1-e). The length and diameter of ZnO NRAs are tunable by varying the zinc nitrate concentration and reaction time during the hydrothermal synthesis step (Luo et al., 2020). The individual ZnO rods (Fig. 1-f) on ZnO NRAs/ACFs show a single crystalline nature (Fig. 1-h) with high crystallinity (Fig. 1-g), which was also confirmed by its powder X-ray diffraction (PXRD) patterns (Luo et al., 2020).

The advantage of this sequential sol-gel and hydrothermal synthesis method to grow ZnO NRAs on flexible ACFs substrates is that the characteristics of the ZnO nanorods, such as growth orientation, rod concentration, aspect ratio (rod length/rod diameter) and surface area of the ZnO NRAs, are controllable by adjusting the two-step synthesis parameters (concentration of zinc acetate (x), zinc nitrate (y) and hydrothermal reaction time (z)). Accordingly, 9 ZnO NRAs/ACFs-x-y-z catalysts were synthesized to investigate the effect of ZnO characteristics (Table 1) on photocatalytic degradation performance.

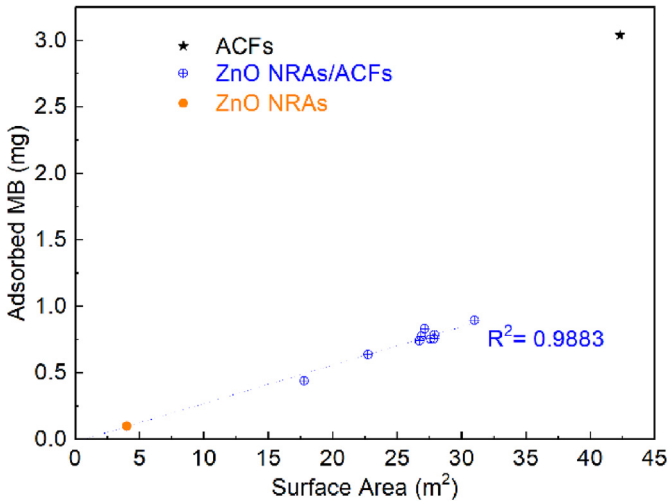

Fig. 2. MB adsorbability for ACFs, ZnO NRAs and ZnO NRAs/ACFs with different surface area.

3.2. Dark adsorption of MB on ZnO NRAs/ACFs

Photocatalytic degradation of methylene blue (a well-known basic dye in the textile industry (Li et al., 2013)) over the ZnO NRAs/ACFs was evaluated in a jacketed glass batch reactor at 25 °C using UV light with a constant illumination intensity as the light source. Photocatalytic degradation of an organic pollutant over heterogeneous photocatalysts (*e.g.*, SiO_2 and ZnO on AC) is generally believed to occur by a two-step mechanism: the organic molecule is first adsorbed on the catalyst surface followed by oxidation by photogenerated active radicals (*e.g.*, hydroxyl radicals). Since the adsorption of the pollutants on the photocatalyst is the prerequisite for catalytic photodegradation (Raizada et al., 2014; Matos et al., 1998), the extent of methylene blue adsorption on the as-prepared ZnO NRAs/ACFs was first considered.

To eliminate the effect of light on the adsorption of dye molecules, the adsorbability of MB on ZnO NRAs/ACFs was tested by performing a dark reaction for 2 h under stirring. Typically, the time to establish adsorption/desorption equilibrium of MB on a catalyst is 30–120 min (Zhang et al., 2014; Melian et al., 2009; Sobana and Swaminathan, 2007; Becker et al., 2011). It can be seen from Table S1 (Entry's 1–9) that almost 30–60% of MB is removed from the aqueous solution by adsorption on ZnO NRAs/ACFs catalysts. Of

Table 1
Characteristics of the ZnO NRAs/ACFs catalysts synthesized at various conditions. Data taken with permission from Ref (Luo et al., 2020).

		Step 1 -sol-gel synthesis	Step 2 -hydrothermal synthesis					
Entry	Catalyst	$Zn(CH_3COO)_2$ (mol L^{-1})	$Zn(NO_3)_2$ (mol L^{-1})	Hydrothermal time (h)	ZnO loading (atom %)	S_{BET} (m^2 g^{-1})[a]	S_{BET} (m^2 g^{-1})[b]	Aspect ratio
1	ZnO NRAs/ACFs-0.10-0.025-4	0.10	0.025	4	7.1	16	689	15:1
2	ZnO NRAs/ACFs-0.15-0.025-4	0.15	0.025	4	10.6	13	619	15:1
3	ZnO NRAs/ACFs-0.20-0.025-4	0.20	0.025	4	19.7	14	505	15:1
4	ZnO NRAs/ACFs-0.25-0.025-4	0.25	0.025	4	21.1	12	395	15:1
5	ZnO NRAs/ACFs-0.15-0.01-4	0.15	0.010	4	8.2	16	620	20:1
6	ZnO NRAs/ACFs-0.15-0.05-4	0.15	0.050	4	16.9	6	603	12:1
7	ZnO NRAs/ACFs-0.15-0.1-4	0.15	0.100	4	18.4	4	594	5:1
8	ZnO NRAs/ACFs-0.15-0.025-3	0.15	0.025	3	9.3	20	613	7.5:1
9	ZnO NRAs/ACFs-0.15-0.025-5	0.15	0.025	5	13.6	5	597	18:1
10	ZnO NRs/ACFs-0-0.025-4	0	0.025	4	8.0	–	–	–
11	ZnO-ACFs	–	–	–	18.1	4	–	–

[a] Surface area of ZnO NRAs peeled off from ZnO NRAs/ACFs.
[b] Surface area of ZnO NRAs/ACFs.

interest is the observation that the adsorbed amount of MB linearly increases with the surface area of the ZnO NRAs/ACFs (Fig. 2). The adsorbability of MB is 0.025–0.031 mg per square meter of ZnO NRAs/ACFs (Table S1), which is almost similar to the MB adsorbability of ZnO NRAs peeled off from the ZnO NRAs/ACFs (*ca.* 0.025 mg MB per square meter of ZnO, Entry 10 in Table S1). Vinayagam et al. (2018) found that the dark adsorption of a dye molecule (orange G) on ZnO catalysts fitted well with a Langmuir equation assuming a homogeneous and monolayer adsorption on the surface. We have illustrated (Luo et al., 2020) that the layer of ZnO nanocrystalline grains was grown on the ACFs surface after the sol-gel synthesis and nucleation and incubation in the initial stage of the hydrothermal synthesis. The surface properties of the ZnO NRAs/ACFs catalysts used mainly arise from the ZnO nanoparticles. Consequently, adsorption of MB on the ZnO NRAs/ACFs also follows a Langmuir isotherm. It needs to be noted that dark adsorption may not represent the actual adsorption of MB on the ZnO NRAs when UV light irradiation is applied. Nevertheless, the adsorbability of MB on ZnO NRAs is approximately 39% of that of ACFs (*ca.* 0.072 mg MB per square meter of ACFs, Entry 11 in Table S1). This is most likely related to the intrinsic adsorption properties (*e.g.*, surface area and porosity) of ZnO and ACFs. It should be highlighted here that the adsorption of dye molecules on ZnO can be remarkably enhanced by increasing its surface area *via* coating on ACFs with a high surface area.

3.3. Effect of ZnO NRAs characteristics on the photocatalytic degradation of MB over ZnO NRAs/ACFs

Photocatalytic degradation studies of MB on ZnO NRAs/ACFs described in this section were all carried out at similar reaction conditions (300 mL MB aqueous solution, initial MB concentration of 5 mg L^{-1}, catalyst dosage of 45 mg, dark adsorption for 2 h and 2 h photodegradation). A preliminary experiment on photodegradation of MB without the use of a catalyst showed a constant MB concentration, indicating that the photodegradation of MB by only applying the UV light for 2 h is negligible. A photosensitization effect may occur when the photocatalyst is present, though is expected to be limited when using ZnO photocatalysts (da Silva et al., 2017) and is therefore not considered in this study.

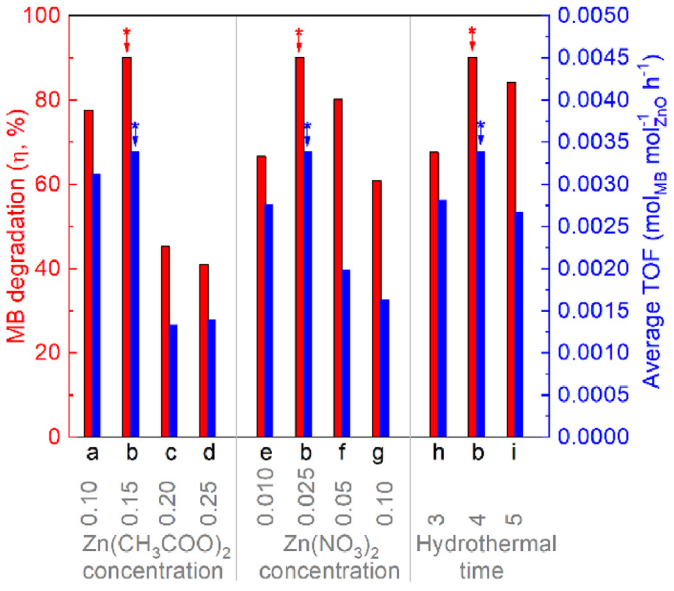

Fig. 3. MB Degradation (η) and average TOF for ZnO NRAs/ACFs catalysts prepared under different sol-gel and hydrothermal synthesis conditions: (a) ZnO NRAs/ACFs-0.10-0.025-4, (b) ZnO NRAs/ACFs-0.15-0.025-4, (c) ZnO NRAs/ACFs-0.20-0.025-4, (d) ZnO NRAs/ACFs-0.25-0.025-4, (e) ZnO NRAs/ACFs-0.15-0.01-4, (f) ZnO NRAs/ACFs-0.15-0.05-4, (g) ZnO NRAs/ACFs-0.15-0.1-4, (h) ZnO NRAs/ACFs-0.15-0.025-3, and (i) ZnO NRAs/ACFs-0.15-0.025-5.

It is difficult to identify whether the reduction in concentration of MB is due to degradation/mineralization or by adsorption. To eliminate the latter, the MB concentration after 2 h dark adsorption was applied as the initial MB concentration and used for calculation of the extent of MB degradation and mineralization (Equations 1-2). The MB concentration and degradation (η) *versus* the photocatalytic reaction time for the various ZnO NRAs/ACFs catalysts are shown in Figs. S1–S3. Rapid photodegradation of MB was observed in the initial stage of the reaction (0–1 h). Afterwards, the degradation rate slowed down gradually. The degradation (η) of MB and average TOF of the ZnO NRAs/ACFs for a 2 h reaction time are plotted in Fig. 3, showing that the photocatalytic performance of the catalysts is highly depending on the ZnO NRAs/ACFs. The most efficient photocatalytic degradation (90.2%) and highest average TOF (0.0034 mol_{MB} mol^{-1}_{ZnO} h^{-1}) were obtained using the ZnO NRAs/ACFs-0.15-0.025-4 (Fig. 3-b). In the subsections below, the relation between ZnO NRAs/ACFs structure (and thus synthesis protocol) and photocatalytic degradation is discussed.

3.3.1. Photocatalytic degradation performance of ZnO NRAs/ACFs catalysts prepared at different sol-gel synthesis conditions

It has been reported by the authors (Luo et al., 2020) that higher concentrations of zinc acetate (from 0.1 to 0.25 mol L^{-1}) for the sol-gel synthesis significantly increases the ZnO nanorods concentration and ZnO loading (7.1–21.1 atom%, Table 1) of the prepared ZnO NRAs/ACFs, without affecting the aspect ratio (15:1, Table 1) and specific surface area (12–16 m^2 g^{-1}, Table 1) of the ZnO NRAs. Fig. 3 shows that a slight increase in the ZnO dosage (from 0.055 g L^{-1} (Fig. 3-a) to 0.071 g L^{-1} (Fig. 3-b)) leads to an increased MB degradation (from 77.5% to 90.2%), which is related to the amount of active sites available for photocatalysis. However, photocatalytic performance is lowered significantly when further increasing the ZnO dosage to 0.113 g L^{-1}, Fig. 3-d. High ZnO dosage may enhance light scattering (Evgenidou et al., 2005) and reduce the penetration (Vinayagam et al., 2018) of light in solution, leading to worse performance. A similar effect on the degradation efficiency (*e.g.*, when using direct blue 53 and acid violet) on ZnO nanoparticles mixed with (Sobana and Swaminathan, 2007) or loaded on (Byrappa et al., 2006) activated carbon was reported as well.

3.3.2. Photocatalytic degradation performance of ZnO NRAs/ACFs prepared at different hydrothermal synthesis conditions

Under the optimized sol-gel conditions (zinc acetate concentration was 0.15 mol L^{-1}), variation of the hydrothermal synthesis conditions (*e.g.*, zinc nitrate concentration and hydrothermal time) led to ZnO NRAs/ACFs with similar surface areas (594–620 m^2 g^{-1}, Table 1) but distinct differences in ZnO nanorods characteristics such as concentration, surface area and aspect ratio (Luo et al., 2020). This allowed us to investigate the effect of the ZnO nanostructure on the photocatalytic degradation of MB at similar concentrations after dark adsorption (2.2–2.5 mg L^{-1}, Figs. S2-I and S3-I). Unfortunately, the number of ZnO NRAs/ACFs catalysts used in this study is limited, which makes it impossible to draw conclusions on the effect of individual structural characteristics such as aspect ratio and surface area. As such, no apparent dependence of the TOF of the ZnO NRAs/ACFs catalysts on the ZnO rods aspect ratio (Fig. 4-a), ZnO rods surface area (Fig. 4-b) and ZnO dosage (Fig. 4-c) was observed, due to the fact that these factors are correlated.

Interestingly, the photoluminescence properties of ZnO NRAs (Fig. 5 and Table S2) seem to be of high importance (Fig. 4-d). The room-temperature photoluminescence spectra of ZnO NRAs (Fig. 5)

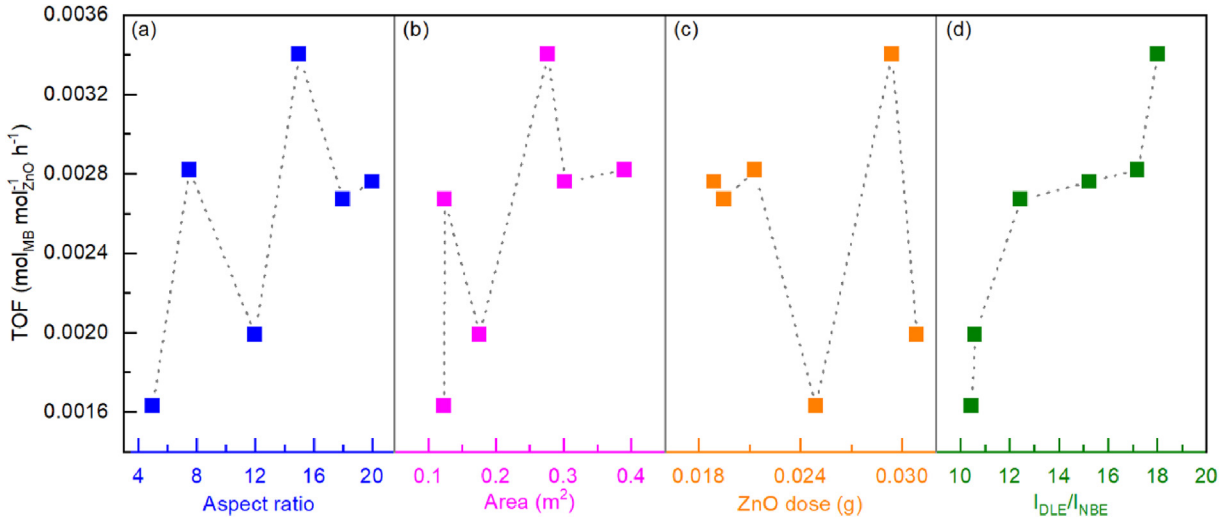

Fig. 4. TOFs of ZnO NRAs/ACFs *vs.* (a) ZnO nanorods aspect ratio, (b) ZnO nanorods surface area, (c) ZnO dosage and (d) the intensity ratio of deep-level emission to near-band-edge emission of ZnO nanorods.

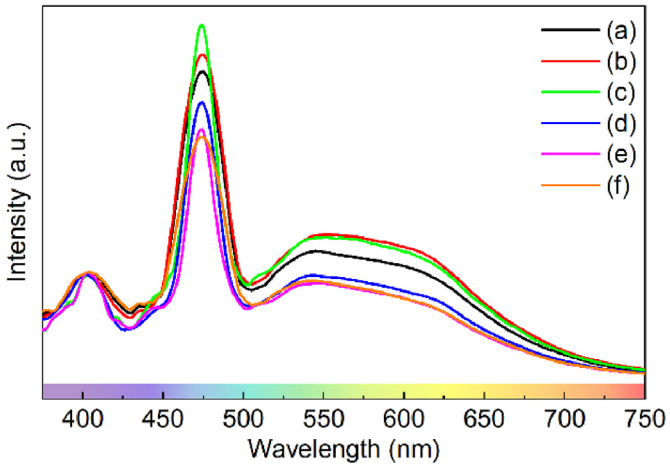

Fig. 5. Photoluminescence spectra of ZnO NRAs peeled off from (a) ZnO NRAs-0.15-0.01-4, (b) ZnO NRAs-0.15-0.025-3, (c) ZnO NRAs-0.15-0.025-4, (d) ZnO NRAs-0.15-0.025-5, (e) ZnO NRAs-0.15-0.05-4, and (f) ZnO NRAs-0.15-0.1-4.

show four emission bands: a weak ultraviolet emission band centered at 405 nm, a sharp blue emission band centered at 475 nm, and a broad green emission band centered at 535 nm with a shoulder from the yellow emission band at 620 nm. The UV emission band, generally centered at 380 nm, is characteristic for the near-band-edge emission (NBE) of a ZnO semiconductor (Giakoumaki et al., 2017), associated with the recombination of excitons (Zeng et al., 2010; Yang et al., 2010; He et al., 2018; Gao et al., 2012). The UV emission band for the ZnO NRAs used in this study is red-shifted to 405 nm (Fig. 5). Such a red-shift was also observed for modified single-crystal ZnO nanowires (from 385 nm to 397 nm) (Deng et al., 2009) and ZnO NRAs (from 375.2 nm to 391.6 nm) (Tan et al., 2016). This shift is believed to be related to a high level of intrinsic Zn defects (*e.g.*, Zn_i and V_{Zn}), which are known to play crucial role in UV emissions in ZnO materials (Rao et al., 2014). According to this, the extended red-shift to 405 nm observed for ZnO NRAs indicates its highly defective nature. The deep-level emissions (DLE) in the visible region are related to intrinsic and extrinsic defects in ZnO, although the defects and the electron transitions are still unambiguous for blue emission (*e.g.*, attributed to the transition from the extended interstitial-zinc (*ex*-Zn_i) state to the valence band (Zeng et al., 2010)), green emission (*e.g.*, due to the recombination of electrons in singly ionized oxygen-vacancy (V_O) with the photoexcited holes (Vanheusden et al., 1996)) and yellow emission (*e.g.*, ascribed to interstitial-oxygen (O_i) defect (Wu et al., 2001)). The intensities of the DLE peaks in photoluminescence spectra normalized on NBE peaks are an indication for the defect levels in ZnO (Zhang et al., 2014). Alternatively, the intensity ratio of the DLE to NBE (I_{DLE}/I_{NBE}) peaks may be used to get a semi-quantitative indication of crystal defects (He et al., 2018; Gao et al., 2012; Pal and Santiago, 2005; Azad et al., 2017). The normalized photoluminescence spectra (Fig. 5) and the calculated I_{DLE}/I_{NBE} ratio (Table S2) of ZnO NRAs clearly show the difference in defect levels for the various ZnO NRAs prepared at different hydrothermal synthesis conditions. A very good correlation between the photocatalytic degradation efficiency (TOF) and catalyst defects (I_{DLE}/I_{NBE}) (Fig. 4-d) was observed and implies that defects (*e.g.*, the two predominant Zn_i and V_O defects) are the active sites of the ZnO catalysts when considering photocatalytic degradation (Zhang et al., 2014). Thus, defects in the ZnO NRAs are likely more important for catalyst performance than other structural properties (*e.g.*, rod concentration, surface area and aspect ratio).

3.4. Synergistic effects between ZnO NRAs and ACFs for the photocatalytic degradation of MB

Several studies revealed a synergistic effect between ZnO nanocrystals and activated carbon or activated carbon fibers in photocatalytic degradation (Melian et al., 2009; Thi and Lee, 2017; Raizada et al., 2014; Byrappa et al., 2006; Sobana and Swaminathan, 2007; Vinayagam et al., 2018; Chen et al., 2014, 2016). However, comparison is cumbersome since other factors, *e.g.*, the initial dye concentration after dark adsorption and ZnO dosage, also play a role and these factors are not always kept at constant values. In our previous report, we observed a synergistic effect between ZnO crystals and ACFs when comparing catalyst performance for experiments with mechanically mixed ZnO-ACFs, ZnO nanorods randomly grown on ACFs (ZnO NRs/ACFs) and ZnO nanorod arrays orderly assembled on ACFs (ZnO NRAs/ACFs). This is clear when considering MB degradation (η) over ACFs mixed/supported ZnO catalysts (Entry's 3, 6 and 9, Table S3) with those for bare ZnO crystals (Entry's 1, 4 and 7, Table S3) (Luo et al., 2020). However, the

performance of the well-aligned ZnO NRAs on ACFs (η of 77.5%, Entry 9, Table S3) is only marginally better than found for mechanically mixed ZnO powder with ACFs (η of 71.6%, Entry 3, Table S3). Comparison though is cumbersome as different ZnO dosages (0.055 g L^{-1} for ZnO NRAs/ACFs *vs*. 0.101 g L^{-1} for ZnO-ACFs) were applied due. Differences in ZnO loading (or ZnO rod concentration) on the catalysts (Table 1) was adjusted to obtain similar MB concentrations after dark adsorption (Luo et al., 2020). To eliminate ZnO dosage effects, turnover frequency of the catalysts was used as a measure to compare the photocatalytic efficiency. Three types of catalysts (ZnO-ACFs (18.1 atom.% Zn, Entry 11, Table 1), ZnO NRs/ACFs-0-0.025-4 (8.0 atom.% Zn, Entry 10, Table 1, termed as ZnO NRs/ACFs hereafter) and ZnO NRAs/ACFs-0.1-0.025-4 (7.1 atom.% Zn, Entry 1, Table 1, termed as ZnO NRAs/ACFs hereafter)), were evaluated, considering that the MB concentrations after dark adsorption for 2 h using these catalysts were similar (*ca.* 2 mg L^{-1}, Table S3).

3.4.1. Photocatalytic degradation performance of ZnO powder, ZnO NRs and ZnO NRAs

To study synergistic effects, ZnO crystals without ACFs, namely ZnO powder, ZnO NRs peeled off from ZnO NRs/ACFs, and ZnO NRAs peeled off from ZnO NRAs/ACFs, were initially evaluated for the photocatalytic degradation of MB. Experiments were carried out at the same initial MB concentration (*ca.* 2 mg L^{-1}), reaction time (120 min or 60 min) and ZnO dosage (0.067 g L^{-1} or 0.833 g L^{-1}). Generally, the use of ZnO crystals at a low ZnO dosage (0.067 g L^{-1}) gave relatively poor MB degradations (η) (Luo et al., 2020) with values of 31.9–47.1% after 120 min (Entry's 1, 4 and 7 in Table S3). Increasing the ZnO dosage to 0.833 g L^{-1} leads to improved MB degradation (84.7–89.9%, Entry's 2, 5 and 8 in Table S3) at an even shorter reaction time of 60 min, related to the higher amount of catalyst used. However, the TOFs of the three types of ZnO crystals decreased with higher ZnO dosage (Table S3). The TOFs of the three types of ZnO crystals at a low ZnO dosage (0.067 g L^{-1}) are plotted in Fig. 6-B.

The TOF found for the 1D ZnO NRs (0.00114 h^{-1}) and ZnO NRAs (0.0015 h^{-1}) is considerably higher than for commercial ZnO powder (0.001 h^{-1}) and this may be ascribed to a higher defect level and enhanced favorable optical properties of the former (Luo et al., 2020). In addition, the unique one-dimensional structure of ZnO crystals might also play an important role in improving light capture (Guo et al., 2012), and enhancing the transport of electrons and thus inhibiting the recombination of photogenerated electron/hole pairs (Lin et al., 2015). Since photocatalytic degradation reactions generally occur on the catalyst surface, the increased surface area for 1D ZnO crystals (16 m^2 g^{-1} for ZnO NRAs *vs*. 4 m^2 g^{-1} for ZnO powder, Table 1) might also be beneficial for catalyst activity. For the 1D ZnO nanocrystals, ZnO NRAs show a higher TOF than ZnO NRs, which might be related to particle anisotropy. Compared to ZnO NRs, ZnO NRAs grow along c-axis, resulting in a higher amount of (002) planes (Luo et al., 2020). This favors the adsorption of OH^-, and as such leads to higher concentrations of OH· radicals and a better photocatalytic degradation efficiency (Dodd et al., 2009). On the other hand, the well-constructed space charge region along the longitudinal direction of ZnO can allow the flow of the photogenerated electrons in the axial direction, which dramatically inhibited the recombination of electron/hole (e^-/h^+) pairs, resulting in large amount of e^- and h^+ on the surface acting as active sites for the intensified photocatalytic degradation efficiency (Zhang et al., 2014).

We have screened the literature and have attempted to determine the TOFs of state-of-the-art ZnO NRs and ZnO NRAs. However, this proved difficult as often not all relevant data is provided (*e.g.*, ZnO dosage). TOF values for a representative ZnO NRs (TOF of 0.00162 h^{-1} (Zhang et al., 2014)) and a ZnO NRAs (TOF of 0.00114 h^{-1} (Song et al., 2012)) were calculated and are given in Table S3 (Entry's 12–13) together with the photocatalytic reaction conditions. It can be seen that the TOFs of the as-synthesized ZnO NRs (0.00139 h^{-1}, Entry 10 in Table S3 and ZnO NRAs (0.00147 h^{-1}, Entry 11 in Table S3) are comparable with state-of-the-art 1D ZnO crystals. Considering that the power of the UV lamp used in this work is only 8 W, which is much lower than those used in the literature (400 W (Zhang et al., 2014) and 300 W (Song et al., 2012), Table S3), the photocatalytic degradation efficiency on the as-synthesized ZnO NRs and ZnO NRAs is expected to be significantly increased when using UV light at a higher power level.

3.4.2. Photocatalytic degradation of MB over ZnO-ACFs, ZnO NRs/ACFs and ZnO NRAs/ACFs

Immobilizing ZnO NRs and NRAs on ACFs as well as mechanically mixed ZnO powder and ACFs catalysts showed significantly enhanced TOFs compared to the corresponding ZnO nanocrystals (Fig. 6-B). This positive effect of the addition of ACFs is clearly seen from the TOFs for ZnO powder (0.001 h^{-1}, Fig. 6-B and Entry 1 in Table S3) and the mixed ZnO-ACFs (0.00183 h^{-1}, Fig. 6-B and Entry

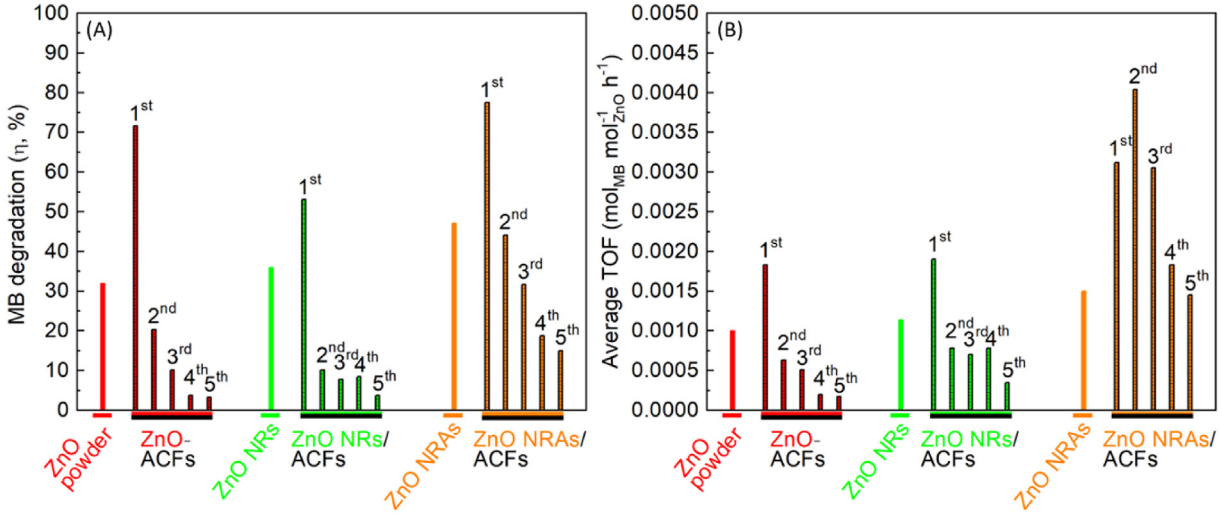

Fig. 6. (A) MB Degradation (η) and (B) average TOF for ZnO-ACFs, ZnO NRs/ACFs-0-0.025-4 and ZnO NRAs/ACFs-0.1-0.025-4 catalysts for 5 successive recycle experiments.

3 in Table S3). ACFs most likely adsorb the dye molecules, which are then transferred to the photoactive ZnO sites (Sobana and Swaminathan, 2007). Comparatively, a better synergistic effect is observed when using ZnO NRAs/ACFs, which showed a TOF (0.00312 h^{-1}, Fig. 6-B and Entry 9 in Table S3) twice as high as for ZnO NRAs (0.0015 h^{-1}, Fig. 6-B and Entry 7 in Table S3). This is most likely related to the enhanced adsorbability of MB (Fig. 2) on ZnO NRAs/ACFs compared to ZnO NRAs, associated with a larger surface area for the former (Table 1) (Raizada et al., 2014). In addition, the high conductivity of ACFs can promote the transport of the photogenerated electrons (Chen et al., 2014, 2016). As a consequence, the photogenerated electron/hole (e^-/h^+) pairs are effectively separated, leading to an efficient generation of the reactive OH· radicals for enhanced photocatalytic degradation efficiency. ZnO NRAs/ACFs showed the highest TOF (0.00312 h^{-1}, Fig. 6-B and Entry 9 in Table S3), which is almost three times the TOF found for commercial ZnO powder (0.001 h^{-1}, Fig. 6-B and Entry 1 in Table S3). This indicates that immobilization of well-aligned ZnO NRAs on flexible ACFs (ZnO NRAs/ACFs) leads to catalysts with outstanding photocatalytic degradation performance when compared to related ZnO based photocatalysts.

Of great interest is the observation that mineralization of MB to CO_2 over ZnO NRAs/ACFs (55.0%, Fig. 7-C) is significantly higher than found for ZnO-ACFs (23.6%, Fig. 7-A). The degradation chemistry of MB is known to be rather complicated and involves a large number of intermediates such as phenolics and carboxylic acids, formed by a series of radical reactions (Wang et al., 2014; Huang et al., 2010). Therefore, the high reduction in TOC over ZnO NRAs/ACFs (Fig. 7-C) also indicates an effective conversion/degradation of intermediates from the photodegradation of MB.

3.4.3. *Reusability (or stability) of ZnO-ACFs, ZnO NRs/ACFs and ZnO NRAs/ACFs for photocatalytic degradation of MB*

It is well known that the separation of ZnO nanocrystals (*e.g.*, as powder, NRs and NRAs) after reaction from the solution is difficult and limits recycling of the catalysts. In addition, catalyst stability is limited due to the formation of aggregates resulting in reduction of active sites and loss of structural integrity and optical properties favorable for photocatalytic degradation (Lu et al., 2008; Thi and Lee, 2017). This is a serious problem and the origin of immobilization of ZnO nanocrystals on a substrate in this study. To check the reusability (or stability) of the three types of catalysts used in this study (ZnO-ACFs, ZnO NRs/ACFs and ZnO NRAs/ACFs), the used catalysts after a photocatalytic degradation were filtered and reused for another experiment following the same protocol as used to evaluate activity of the fresh catalysts. In total, the catalysts were used for 5 times. The concentrations and degradations (η) of MB *versus* reaction time are tabulated in Table S4, and the degradation of MB and TOF for the fresh and used catalysts are shown in Fig. 6.

The mechanically mixed ZnO-ACFs showed very poor reusability (or stability), of which the TOF was only 9.5% of the original value after 5 recycles (Fig. 6-B and S9, Entry's 6–10 in Table S4). This is mostly related to the loss of ZnO during the tedious work-up procedure (Raizada et al., 2014). ZnO NRs/ACFs catalysts showed slightly better recyclability as compared to ZnO-ACFs (Fig. 6-B and Entry's 11–15 in Table S4). The TOF of ZnO NRs/ACFs after recycling 5 times decreased to 18.3% of the initial TOF. It was observed that the ZnO nanorods and microspheres (Fig. 1) of the ZnO NRs/ACFs were not stable and readily peeled off during photocatalytic degradation of MB (Luo et al., 2020). As such, the synergistic effect between ZnO NRs and ACFs was lost significantly even after 1 recycle resulting in a dramatic reduction (*ca.* 60%) in the TOF. Comparatively, ZnO NRAs/ACFs showed promising reusability (or stability, Fig. 6-B and Entry's 16–20 in Table S4). After 1 recycle, a higher TOF (0.00404 h^{-1} *vs.* 0.00312 h^{-1}, Fig. 6-B and Entry 17 *vs.* 16 in Table S4) was observed, which might be due to a higher initial MB concentration after the dark adsorption step (4.60 mg L^{-1} *vs.* 2.01 mg L^{-1}, Entry 17 *vs.* 16 in Table S4) (Yuan et al., 2007). Nevertheless, the TOF of ZnO NRAs/ACFs decreased gradually with more recycles, likely due to poisoning of the ZnO surface by strongly adsorbed intermediates (Raizada et al., 2014). The TOF of MB over ZnO NRAs/ACFs after 5 recycles (0.00145 h^{-1}, Fig. 6-B and Entry 20 in Table S4) was reduced to 46.5% of that of the fresh catalyst. However, it needs to be highlighted that this TOF is still comparable with that of the fresh ZnO NRAs (0.00147 h^{-1}, Entry 11 in Table S3). Therefore, the synergistic effect between ACFs and the immobilized 1D ZnO NRAs is not only reflected by a significantly enhanced TOF for the photocatalytic degradation of MB, but also by a better catalyst reusability (or stability). The latter may also be attributed to a reduced level of photocorrosion of the ZnO nanoparticles in the presence of ACFs (Zhang et al., 2009).

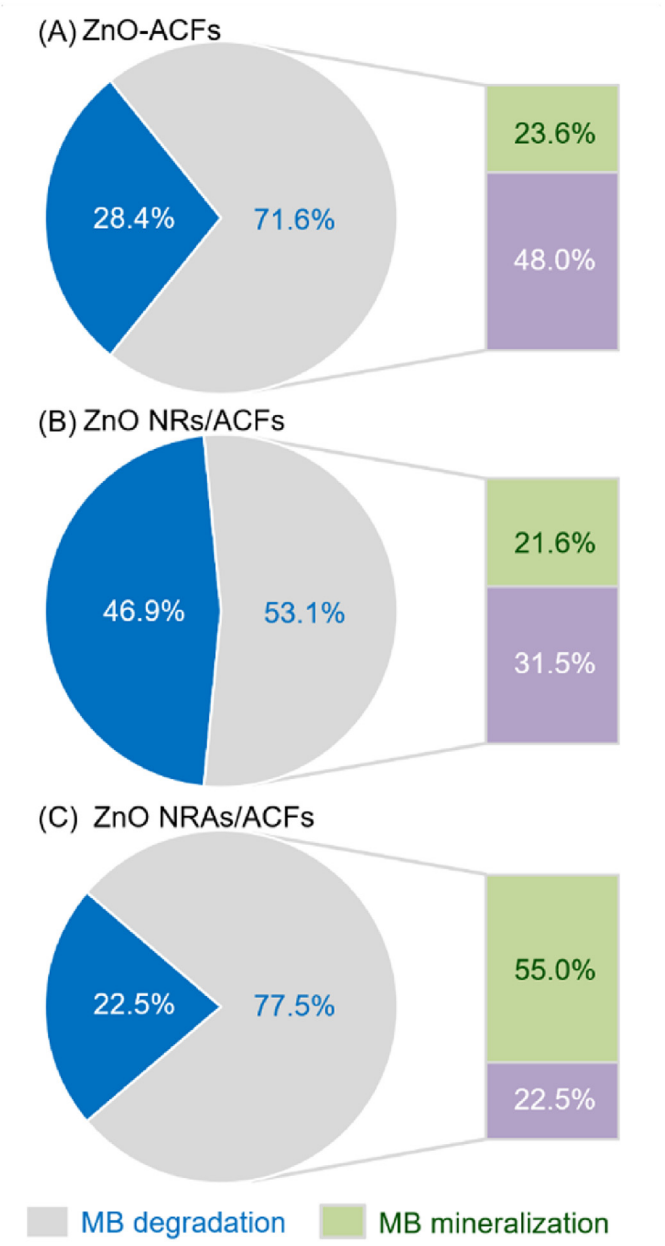

Fig. 7. MB degradation and mineralization over ZnO-ACFs, ZnO NRs/ACFs-0-0.025-4 and ZnO NRAs/ACFs-0.1-0.025-4 catalysts.

4. Conclusions

In summary, well-aligned single-crystal ZnO nanorod arrays on activated carbon fibers were synthesized by a sequential sol-gel and hydrothermal synthesis method. The as-synthesized ZnO NRAs show excellent MB adsorbability (*ca*. 0.025 mg MB per square meter of ZnO) in the dark, which is approximately 39% of that found for the pristine ACFs. The amount of MB adsorbed on ZnO NRAS/ACFs in the dark increases linearly with the surface area of the catalysts, in line with a Langmuir adsorption.

The defect level as determined by photoluminescence is an important property of the catalysts and has a larger effect on catalytic activity than aspect ratio, surface area and dosage. ZnO NRAs show higher TOF (0.0015 mol_{MB} mol_{ZnO}^{-1} h^{-1}) than a commercial ZnO powder (0.001 mol_{MB} mol_{ZnO}^{-1} h^{-1}), associated with the unique one-dimensional and highly oriented structure, higher surface area and particularly a higher defect level of the ZnO NRAs.

A significant improvement in photocatalytic degradation performance was obtained when immobilizing the ZnO NRAs on ACFs (TOF of 0.00312 mol_{MB} mol_{ZnO}^{-1} h^{-1}), indicating a synergistic effect, which is higher than for a mechanically mixed ZnO-ACFs catalyst (TOF of 0.00183 mol_{MB} mol_{ZnO}^{-1} h^{-1}). This synergistic effect might be related to enhanced MB adsorption and a faster transfer of the photogenerated electrons.

ZnO NRAs/ACFs show a significantly higher mineralization of MB than the mixed ZnO-ACFs (55.0% *vs*. 23.6%). Besides, reusability (or stability) for ZnO NRAs/ACFs after 5 recycles is also considerably better than for the mixed ZnO-ACFs, indicating the advantage of immobilization of ZnO nanorod arrays on ACFs for catalyst reuse. This work has shown that the assembly of ZnO NRAs on ACFs is highly beneficial for enhanced photocatalytic degradation performance.

Author contribution

Sha Luo: Conceptualization, Methodology, Validation, Writing - original draft, Writing - review & editing, Chunwei Liu: Investigation. Sui Zhou: Investigation. Wei Li: Resources, Data curation, Project administration, Chunhui Ma: Investigation, Validation, Shouxin Liu: Supervision, Project administration, Funding acquisition, Writing - review & editing. Wang Yin: Investigation. Hero Jan Heeres: Supervision, Writing - review & editing. Weiqing Zheng: Investigation. Kulathuiyer Seshan: Supervision, Writing - review & editing. Songbo He: Conceptualization, Visualization, Supervision, Writing - original draft, Writing - review & editing.

Declaration of competing interest

The authors declare that they have no known competing financial interests or personal relationships that could have appeared to influence the work reported in this paper.

Acknowledgments

We thank National Key R&D Program of China (Grant No. 2017YFD0601006) and Fundamental Research Funds for the Central Universities (Grant No. 2572016BB02) for their financial support.

Appendix A. Supplementary data

Supplementary data to this article can be found online at https://doi.org/10.1016/j.chemosphere.2020.127731.

References

Al Haiqi, O., Nour, A.H., Bargaa, R., Ayodele, B.V., 2020. Effect of process parameters on the photocatalytic degradation of phenol in oilfield produced wastewater using ZnO/Fe_2O_3 nanocomposites. Bull. Chem. React. Eng. Catal. 15, 128–136. https://doi.org/10.9767/bcrec.15.1.6068.128-136.

Azad, P.F., Naderi, N., Eshraghi, M.J., Massoudi, A., 2017. The effect of seed layer on optical and structural characteristics of ZnO nanorod arrays deposited by CBD method. J. Mater. Sci. Mater. Electron. 28, 15495–15499. https://doi.org/10.1007/s10854-017-7437-x.

Becker, J., Raghupathi, K.R., St Pierre, J., Zhao, D., Koodali, R.T., 2011. Tuning of the crystallite and particle sizes of ZnO nanocrystalline materials in solvothermal synthesis and their photocatalytic activity for dye degradation. J. Phys. Chem. C 115, 13844–13850. https://doi.org/10.1021/jp2038653.

Bojer, C., Schobel, J., Martin, T., Ertl, M., Schmalz, H., Breu, J., 2017. Clinical wastewater treatment: photochemical removal of an anionic antibiotic (ciprofloxacin) by mesostructured high aspect ratio ZnO nanotubes. Appl. Catal., B 204, 561–565. https://doi.org/10.1016/j.apcatb.2016.12.003.

Byrappa, K., Subramani, A.K., Ananda, S., Rai, K.M.L., Sunitha, M.H., Basavalingu, B., Soga, K., 2006. Impregnation of ZnO onto activated carbon under hydrothermal conditions and its photocatalytic properties. J. Mater. Sci. 41, 1355–1362. https://doi.org/10.1007/s10853-006-7341-x.

Chakrabarti, S., Dutta, B.K., 2004. Photocatalytic degradation of model textile dyes in wastewater using ZnO as semiconductor catalyst. J. Hazard Mater. 112, 269–278. https://doi.org/10.1016/j.jhazmat.2004.05.013.

Chen, G.H., Wang, Y., Shen, Q.H., Song, Y.J., Chen, G.L., Yang, H., 2014. Synthesis and enhanced photocatalytic activity of 3D flowerlike ZnO microstructures on activated carbon fiber. Mater. Lett. 123, 145–148. https://doi.org/10.1016/j.matlet.2014.03.029.

Chen, G.H., Wang, Y., Dai, G.L., Zhang, F.M., 2016. Immobilization of flower-like ZnO on activated carbon fibre as recycled photocatalysts. Res. Chem. Intermed. 42, 8227–8237. https://doi.org/10.1007/s11164-016-2591-y.

da Silva, G., Carvalho, K.T.G., Lopes, O.F., Gomes, E.S., Malagutti, A.R., Mastelaro, V.R., Ribeiro, C., Mourao, H., 2017. Synthesis of ZnO nanoparticles assisted by N sources and their application in the photodegradation of organic contaminants. ChemCatChem 9, 3795–3804. https://doi.org/10.1002/cctc.201700756.

Deng, Y., Wang, G.S., Li, N., Guo, L., 2009. Synthesis and red-shifted photoluminescence of single-crystalline ZnO nanowires. J. Lumin. 129, 55–58. https://doi.org/10.1016/j.jlumin.2008.07.016.

Dodd, A., McKinley, A., Tsuzuki, T., Saunders, M., 2009. Tailoring the photocatalytic activity of nanoparticulate zinc oxide by transition metal oxide doping. Mater. Chem. Phys. 114, 382–386. https://doi.org/10.1016/j.matchemphys.2008.09.041.

Evgenidou, E., Fytianos, K., Poulios, I., 2005. Semiconductor-sensitized photodegradation of dichlorvos in water using TiO_2 and ZnO as catalysts. Appl. Catal., B 59, 81–89. https://doi.org/10.1016/j.apcatb.2005.01.005.

Fan, F.L., Wang, X.Q., Ma, Y.X., Fu, K., Yang, Y., 2015. Enhanced photocatalytic degradation of dye wastewater using ZnO/reduced graphene oxide hybrids. Fullerenes, Nanotub. Carbon Nanostruct. 23, 917–921. https://doi.org/10.1080/1536383x.2015.1013187.

Feng, T., Feng, G.S., Yan, L., Pan, J.H., 2014. One-dimensional nanostructured TiO_2 for photocatalytic degradation of organic pollutants in wastewater. Int. J. Photoenergy. https://doi.org/10.1155/2014/563879.

Gao, S., Li, D., Li, Y., Lv, X., Wang, J., Li, H., Yu, Q., Guo, F., Zhao, L., 2012. Growth and characterization of ZnO nanorod arrays on boron-doped diamond films by low temperature hydrothermal reaction. J. Alloys Compd. 539, 200–204. https://doi.org/10.1016/j.jallcom.2012.05.096.

Giakoumaki, A.N., Kenanakis, G., Klini, A., Androulidaki, M., Viskadourakis, Z., Farsari, M., Selimis, A., 2017. 3D micro-structured arrays of ZnO nanorods. Sci. Rep. 7, 9. https://doi.org/10.1038/s41598-017-02231-z.

Guo, W.X., Zhang, F., Lin, C.J., Wang, Z.L., 2012. Direct growth of TiO_2 nanosheet arrays on carbon fibers for highly efficient photocatalytic degradation of methyl orange. Adv. Mater. 24, 4761–4764. https://doi.org/10.1002/adma.201201075.

He, G.N., Huang, B., He, Q.Y., Li, L.X., 2018. One-step low-temperature synthesis of syringe-shaped ZnO nanorod arrays, growth mechanism and optical properties. Cryst. Res. Technol. 53 https://doi.org/10.1002/crat.201700283.

Huang, F., Chen, L., Wang, H., Yan, Z., 2010. Analysis of the degradation mechanism of methylene blue by atmospheric pressure dielectric barrier discharge plasma. Chem. Eng. J. 162, 250–256. https://doi.org/10.1016/j.cej.2010.05.041.

Lam, S.M., Kee, M.W., Sin, J.C., 2018a. Influence of PVP surfactant on the morphology and properties of ZnO micro/nanoflowers for dye mixtures and textile wastewater degradation. Mater. Chem. Phys. 212, 35–43. https://doi.org/10.1016/j.matchemphys.2018.03.002.

Lam, S.M., Low, X.Z.D., Wong, K.A., Sin, J.C., 2018b. Sequencing coagulation-photodegradation treatment of Malachite Green dye and textile wastewater through ZnO micro/nanoflowers. Chem. Eng. Commun. 205, 1143–1156. https://doi.org/10.1080/00986445.2018.1434163.

Li, Y.H., Du, Q.J., Liu, T.H., Peng, X.J., Wang, J.J., Sun, J.K., Wang, Y.H., Wu, S.L., Wang, Z.H., Xia, Y.Z., Xia, L.H., 2013. Comparative study of methylene blue dye adsorption onto activated carbon, graphene oxide, and carbon nanotubes. Chem. Eng. Res. Des. 91, 361–368. https://doi.org/10.1016/j.cherd.2012.07.007.

Lin, J.L., Wang, D.F., Chen, D., Ge, Q.S., Ping, G.X., Fan, M.Q., Qin, L.S., Shu, K.Y., 2015. Preparation and enhanced photocatalytic performance of one-dimensional ZnO nanorods. Environ. Prog. Sustain. Energy 34, 74–80. https://doi.org/10.1002/ep.11957.

Liu, R.F., Li, W.B., Peng, A.Y., 2018. A facile preparation of TiO_2/ACF with CTi bond and abundant hydroxyls and its enhanced photocatalytic activity for formaldehyde removal. Appl. Surf. Sci. 427, 608–616. https://doi.org/10.1016/j.apsusc.2017.07.209.

Lu, F., Cai, W.P., Zhang, Y.G., 2008. ZnO hierarchical micro/nanoarchitectures: solvothermal synthesis and structurally enhanced photocatalytic performance. Adv. Funct. Mater. 18, 1047–1056. https://doi.org/10.1002/adfm.200700973.

Luo, S., Liu, C., Wan, Y., Li, W., Ma, C., Liu, S., Jan Heeres, H., Zheng, W., Seshan, K., He, S., 2020. Self-assembly of single-crystal ZnO nanorod arrays on flexible activated carbon fibers substrates and the superior photocatalytic degradation activity. Appl. Surf. Sci. 513 https://doi.org/10.1016/j.apsusc.2020.145878.

Lv, Y.Y., Yu, L.S., Li, C.G., Yang, L.S., 2016. ZnO nanopowders and their excellent solar light/UV photocatalytic activity on degradation of dye in wastewater. Sci. China Chem. 59, 142–149. https://doi.org/10.1007/s11426-015-5438-2.

Marathe, S.D., Shrivastava, V.S., 2015. Removal of hazardous Ponceau S dye from industrial wastewater using nano-sized ZnO. Desalin. Water Treat. 54, 2036–2040. https://doi.org/10.1080/19443994.2014.896293.

Matos, J., Laine, J., Herrmann, J.-M., 1998. Synergy effect in the photocatalytic degradation of phenol on a suspended mixture of titania and activated carbon. Appl. Catal., B 18, 281–291. https://doi.org/10.1016/S0926-3373(98)00051-4.

McLaren, A., Valdes-Solis, T., Li, G.Q., Tsang, S.C., 2009. Shape and size effects of ZnO nanocrystals on photocatalytic activity. J. Am. Chem. Soc. 131, 12540–12541. https://doi.org/10.1021/ja9052703.

Mechiakh, R., Sedrine, N.B., Chtourou, R., Bensaha, R., 2010. Correlation between microstructure and optical properties of nano-crystalline TiO_2 thin films prepared by sol–gel dip coating. Appl. Surf. Sci. 257, 670–676. https://doi.org/10.1016/j.apsusc.2010.08.008.

Melian, E.P., Diaz, O.G., Rodriguez, J.M.D., Colon, G., Arana, J., Melian, J.H., Navio, J.A., Pena, J.P., 2009. ZnO activation by using activated carbon as a support: characterisation and photoreactivity. Appl. Catal., A 364, 174–181. https://doi.org/10.1016/j.apcata.2009.05.042.

Modirshahla, N., Hassani, A., Behnajady, M.A., Rahbarfam, R., 2011. Effect of operational parameters on decolorization of Acid Yellow 23 from wastewater by UV irradiation using ZnO and ZnO/SnO_2 photocatalysts. Desalination 271, 187–192. https://doi.org/10.1016/j.desal.2010.12.027.

Mustapha, S., Ndamitso, M.M., Abdulkareem, A.S., Tijani, J.O., Shuaib, D.T., Ajala, A.O., Mohammed, A.K., 2020. Application of TiO_2 and ZnO nanoparticles immobilized on clay in wastewater treatment: a review. Appl. Water Sci. 10 https://doi.org/10.1007/s13201-019-1138-y.

Nguyen, V.Q., Baynosa, M.L., Nguyen, V.H., Tuma, D., Lee, Y.R., Shim, J.J., 2019. Solvent-driven morphology-controlled synthesis of highly efficient long-life ZnO/graphene nanocomposite photocatalysts for the practical degradation of organic wastewater under solar light. Appl. Surf. Sci. 486, 37–51. https://doi.org/10.1016/j.apsusc.2019.03.262.

Ohyama, M., Kozuka, H., Yoko, T., 1997. Sol-gel preparation of ZnO films with extremely preferred orientation along (002) plane from zinc acetate solution. Thin Solid Films 306, 78–85. https://doi.org/10.1016/s0040-6090(97)00231-9.

Pal, U., Santiago, P., 2005. Controlling the morphology of ZnO nanostructures in a low-temperature hydrothermal process. J. Phys. Chem. B 109, 15317–15321. https://doi.org/10.1021/jp052496i.

Panthi, G., Park, M., Kim, H.Y., Lee, S.Y., Park, S.J., 2015. Electrospun ZnO hybrid nanofibers for photodegradation of wastewater containing organic dyes: a review. J. Ind. Eng. Chem. 21, 26–35. https://doi.org/10.1016/j.jiec.2014.03.044.

Park, S., Park, H.J., Yoo, K., Lee, J.H., Lee, J.C., 2007. Photocatalytic recovery of Ag ions from wastewater using ZnO nanopowders immobilized on microporous alumina substrates. Colloid. Surface. Physicochem. Eng. Aspect. 300, 30–34. https://doi.org/10.1016/j.colsurfa.2006.10.020.

Raizada, P., Singh, P., Kumar, A., Sharma, G., Pare, B., Jonnalagadda, S.B., Thakur, P., 2014. Solar photocatalytic activity of nano-ZnO supported on activated carbon or brick grain particles: role of adsorption in dye degradation. Appl. Catal., A 486, 159–169. https://doi.org/10.1016/j.apcata.2014.08.043.

Raj, R.B., Umadevi, M., Parimaladevi, R., 2019. Enhanced photocatalytic degradation of textile dyeing wastewater under UV and visible light using ZnO/MgO nanocomposites as a novel photocatalyst. Part. Sci. Technol. 1–9 https://doi.org/10.1080/02726351.2019.1616863.

Rao, T.P., Goswami, G.K., Nanda, K.K., 2014. Detailed understanding of the excitation-intensity dependent photoluminescence of ZnO materials: role of defects. J. Appl. Phys. 115 https://doi.org/10.1063/1.4881779.

Sobana, N., Swaminathan, M., 2007. Combination effect of ZnO and activated carbon for solar assisted photocatalytic degradation of Direct Blue 53. Sol. Energy Mater. Sol. Cells 91, 727–734. https://doi.org/10.1016/j.solmat.2006.12.013.

Song, L.M., Zhang, S.J., Wu, X.Q., Wei, Q.W., 2012. Controllable synthesis of hexagonal, bullet-like ZnO microstructures and nanorod arrays and their photocatalytic property. Ind. Eng. Chem. Res. 51, 4922–4926. https://doi.org/10.1021/ie202253a.

Tafreshi, N., Sharifnia, S., Dehaghi, S.M., 2019. Photocatalytic treatment of a multi-component petrochemical wastewater by floatable ZnO/Oak charcoal composite: optimization of operating parameters. J. Environ. Chem. Eng. 7, 11. https://doi.org/10.1016/j.jece.2019.103397.

Tan, S.T., Tan, C.H., Chong, W.Y., Yap, C.C., Umar, A.A., Ginting, R.T., Lee, H.B., Lim, K.S., Yahaya, M., Salleh, M.M., 2016. Microwave-assisted hydrolysis preparation of highly crystalline ZnO nanorod array for room temperature photoluminescence-based CO gas sensor. Sens. Actuators, B 227, 304–312. https://doi.org/10.1016/j.snb.2015.12.058.

Thi, V.H.T., Lee, B.K., 2017. Great improvement on tetracycline removal using ZnO rod-activated carbon fiber composite prepared with a facile microwave method. J. Hazard Mater. 324, 329–339. https://doi.org/10.1016/j.jhazmat.2016.10.066.

Tian, M.-J., Liao, F., Ke, Q.-F., Guo, Y.-J., Guo, Y.-P., 2017. Synergetic effect of titanium dioxide ultralong nanofibers and activated carbon fibers on adsorption and photodegradation of toluene. Chem. Eng. J. 328, 962–976. https://doi.org/10.1016/j.cej.2017.07.109.

Ummartyotin, S., Pechyen, C., 2016. Role of ZnO on nylon 6 surface and the photocatalytic efficiency of methylene blue for wastewater treatment. Colloid Polym. Sci. 294, 1217–1224. https://doi.org/10.1007/s00396-016-3881-z.

Vaiano, V., Iervolino, G., 2018. Facile method to immobilize ZnO particles on glass spheres for the photocatalytic treatment of tannery wastewater. J. Colloid Interface Sci. 518, 192–199. https://doi.org/10.1016/j.jcis.2018.02.033.

Vanheusden, K., Warren, W.L., Seager, C.H., Tallant, D.R., Voigt, J.A., Gnade, B.E., 1996. Mechanisms behind green photoluminescence in ZnO phosphor powders. J. Appl. Phys. 79, 7983–7990. https://doi.org/10.1063/1.362349.

Vayssieres, L., 2003. Growth of arrayed nanorods and nanowires of ZnO from aqueous solutions. Adv. Mater. 15, 464–466. https://doi.org/10.1002/adma.200390108.

Vinayagam, M., Ramachandran, S., Ramya, V., Sivasamy, A., 2018. Photocatalytic degradation of Orange G dye using ZnO/biomass activated carbon nanocomposite. J. Environ. Chem. Eng. 6, 3726–3734. https://doi.org/10.1016/j.jece.2017.06.005.

Wang, J.C., Liu, P., Fu, X.Z., Li, Z.H., Han, W., Wang, X.X., 2009. Relationship between oxygen defects and the photocatalytic property of ZnO nanocrystals in Nafion membranes. Langmuir 25, 1218–1223. https://doi.org/10.1021/la803370z.

Wang, Q., Tian, S.L., Ning, P., 2014. Degradation mechanism of methylene blue in a heterogeneous fenton-like reaction catalyzed by ferrocene. Ind. Eng. Chem. Res. 53, 643–649. https://doi.org/10.1021/ie403402q.

Wu, X.L., Siu, G.G., Fu, C.L., Ong, H.C., 2001. Photoluminescence and cathodoluminescence studies of stoichiometric and oxygen-deficient ZnO films. Appl. Phys. Lett. 78, 2285–2287. https://doi.org/10.1063/1.1361288.

Xu, X.L., Jia, Y.M., Xiao, L.B., Wu, Z., 2018. Strong vibration-catalysis of ZnO nanorods for dye wastewater decolorization via piezo-electro-chemical coupling. Chemosphere 193, 1143–1148. https://doi.org/10.1016/j.chemosphere.2017.11.116.

Yang, J.H., Zheng, J.H., Zhai, H.J., Yang, X.M., Yang, L.L., Liu, Y., Lang, J.H., Gao, M., 2010. Oriented growth of ZnO nanostructures on different substrates via a hydrothermal method. J. Alloys Compd. 489, 51–55. https://doi.org/10.1016/j.jallcom.2009.08.159.

Yuan, R.S., Guan, R.B., Liu, P., Zheng, J.T., 2007. Photocatalytic treatment of wastewater from paper mill by TiO_2 loaded on activated carbon fibers. Colloid. Surface. Physicochem. Eng. Aspect. 293, 80–86. https://doi.org/10.1016/j.colsurfa.2006.07.010.

Zeng, H.B., Duan, G.T., Li, Y., Yang, S.K., Xu, X.X., Cai, W.P., 2010. Blue luminescence of ZnO nanoparticles based on non-equilibrium processes: defect origins and emission controls. Adv. Funct. Mater. 20, 561–572. https://doi.org/10.1002/adfm.200901884.

Zhang, L.W., Cheng, H.Y., Zong, R.L., Zhu, Y.F., 2009. Photocorrosion suppression of ZnO nanoparticles via hybridization with graphite-like carbon and enhanced photocatalytic activity. J. Phys. Chem. C 113, 2368–2374. https://doi.org/10.1021/jp807778r.

Zhang, X.Y., Qin, J.Q., Xue, Y.N., Yu, P.F., Zhang, B., Wang, L.M., Liu, R.P., 2014. Effect of aspect ratio and surface defects on the photocatalytic activity of ZnO nanorods. Sci. Rep. 4 https://doi.org/10.1038/srep04596.

Zhang, Z., Song, Y.X., Wu, S., Guo, J.L., Zhang, Q., Wang, J.S., Yang, J.H., Hua, Z., Lang, J.H., 2019. Tuning the defects and luminescence of ZnO:(Er, Sm) nanoflakes for application in organic wastewater treatment. J. Mater. Sci. Mater. Electron. 30, 15869–15879. https://doi.org/10.1007/s10854-019-01911-y.